New results in the analysis of ^{16}O+^{28}Si elastic scattering by modifying the optical potential

I. Boztosun

Department of Physics, Erciyes University, 38039 Kayseri, Turkey

The elastic scattering of the ^{16}O+^{28}Si system has been analyzed with a modified potential within the framework of the optical model over a wide energy range in the laboratory system from 29.0 to 142.5 MeV. This system has been extensively studied over the years and a number of serious problems has remained unsolved: The explanation of the anomalous large angle scattering data; the out-of-phase problem between theoretical predictions and experimental data; the reproduction of the oscillatory structure near the Coulomb barrier; and the consistent description of angular distributions together with the excitation functions data. These are just some of the problems. We propose the use of a modified potential method to explain these problems over this wide energy range. This new method consistently improves the agreement with the experimental data and achieves a major improvement on all the previous optical model calculations for this system.

I. INTRODUCTION

Elastic and inelastic scattering between heavy ions have been among the main sources of information about complex nuclei over the last 40 years. [1–3]. There have been numerous experimental investigations of the systems with a combined mass number of $A_P + A_T \lesssim 60$, and these investigations have displayed a common unexpected feature near $\theta_{CM} = 180°$ for the elastic and inelastic scattering cross sections.

The physical origin of the observed structure is not yet fully understood [2,4–8] and presents a challenge to different approaches that have been proposed to provide its explanation. These approaches range from the occurrence of possibly overlapping shape resonances [9] and the scattering from surface-transparent optical potentials [10] to more exotic effects such as explicit parity dependence of the ion-ion potential [11,12]. The first approach that has been more popular with researchers so far attempts to describe the data by invoking the properties of the average optical potential [10,13–19]. On the other hand, in the second approach, the structure in the excitation function is associated with isolated or nearly isolated partial-wave resonances superimposed on the scattering properties of a standard optical potential [1,2]. At present, none of these approaches provides a consistent explanation for all the existing data for this system.

Consequently, the following problems continue to exist for this reaction [5,8,20,21]: (i) The explanation of anomalous large angle scattering data, (ii) the reproduction of the oscillatory structure near the Coulomb barrier, (iii) the out-of-phase problem between theoretical predictions and experimental data, and (iv) the consistent description of angular distributions together with the excitation functions data.

Within the framework of the coupled-channels method, we have analyzed such light heavy-ion reactions that pose the above-mentioned problems [5,8,20,21]. The new approach that we proposed within the coupled-channels method has successfully explained the experimental data over wide energy ranges for different systems such as ^{12}C+^{12}C, ^{16}O+^{28}Si, ^{16}O+^{24}Mg, and ^{12}C+^{24}Mg. One feature we observed in these analyses was that these reactions were extremely sensitive to the shape of the nuclear potential in the surface region. In this paper, by taking this feature into account, we consider an extensive investigation of the elastic scattering of this system at numerous energies by using a modified potential. Similar to the previously conducted coupled-channels analyses for such systems [5,8,20,21], this new technique modifies the shape of the potential at the surface. Thus, we aim to address the above-mentioned problems within the framework of the optical model and obtain results that are as good as the results of the coupled-channels method. Accordingly, we analyze the experimental data from 29.0 to 142.5 MeV in the laboratory system over the whole angular range up to 180°. The 180° elastic scattering excitation function has also been studied over this energy range. An extensively modified version of the code *CHUCK* [22] has been used for the all calculations.

In the next section, we introduce our optical model and potential parameters to explain the observed experimental data. Then, we show the results of these analyses in Sec. III from $E_{Lab} = 29.0$ MeV to 142.5 MeV. Our conclusion is given in Sec. IV.

II. THE MODEL

The standard optical model with folding model potentials or with similar phenomenological potentials such as the square of the Woods-Saxon has failed to describe certain aspects of the experimental data. Therefore, similar to Mackintosh, Kobos, and Satchler's work [17–19], in the present calculations, our total real potential consists of the nuclear potential, $V_{nuclear}$, with two small additional potentials, $[U(r) = U_1(r) + U_2(r)]$:

$$V_{total}(r) = \underbrace{V_{nuclear}(r) + U(r)}_{real\ potential} + V_{Coulomb}(r) + V_{centrif.}(r).$$

(1)

The nuclear potential is assumed to have the square of a Woods-Saxon shape and the parameters are fixed to reproduce the folding model potential of Mackintosh, Kobos, and Satchler [17–19]:
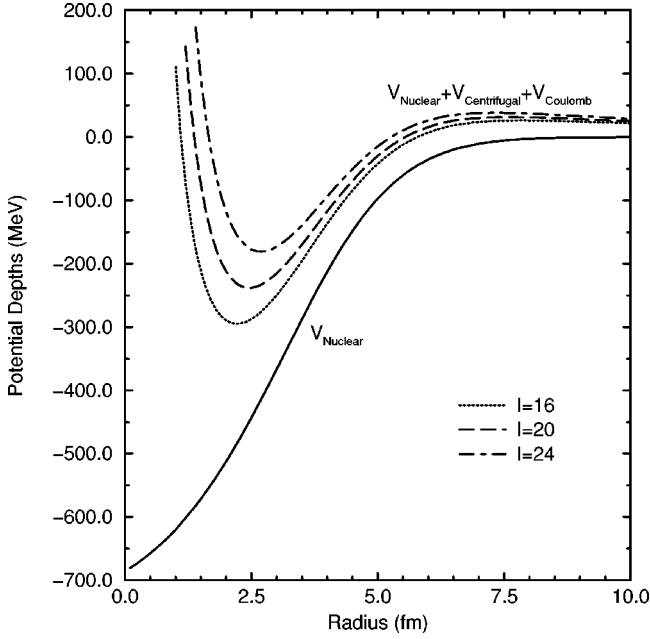
FIG. 1. Interaction potential between ^{16}O and ^{28}Si is plotted against the separation R for various values of the orbital angular momentum quantum number, l. The parameters are given in the text.

$$V_{nuclear}(r) = \frac{-V_0}{[1+\exp(r-R)/a]^2}, \qquad (2)$$

where $V_0 = 761.5$ MeV and $R = r_0(A_a^{1/3} + A_A^{1/3})$ with $r_0 = 0.75$ fm and $a = 1.425$ fm. The parameters of the nuclear potential are fixed as a function of energy and kept constant in the present calculations although small changes were observed to improve the quality of the fits.

The Coulomb potential [23] due to a charge $Z_a e$ interacting with a charge $Z_A e$, distributed uniformly over a sphere of radius R_c, is also added,

$$V_{Coulomb}(r) = \frac{1}{4\pi\epsilon_o} \frac{Z_a Z_A e^2}{r} \qquad r \geq R_c \qquad (3)$$

$$= \frac{1}{4\pi\epsilon_o} \frac{Z_a Z_A e^2}{2R_c} \left(3 - \frac{r^2}{R_c^2}\right) \qquad r < R_c, \qquad (4)$$

where $R_c = 7.78$ fm is the Coulomb radius, and Z_a and Z_A denote the charges of the projectile a and the target nuclei A, respectively.

The sum of the nuclear, Coulomb, and the centrifugal potentials is shown in Fig. 1 for various values of the orbital angular momentum. The superposition of the attractive and repulsive potentials results in the formation of a potential pocket. The width and depth of the pocket depend on the orbital angular momentum quantum number for a given nuclear potential. This pocket is very important for the interference of the barrier and internal waves, which creates the oscillatory structure observed in the cross section.

The significance of the two small additional potentials should be emphasized here, since without them, it would be impossible to fit the experimental data in the elastic scattering calculations. These two small additional potentials are the derivatives of the Woods-Saxon shape and the parameters are shown in Table I where

$$U(r) = 4U_1 a_1 df(r,R_1,a_1)/dr + 4U_2 a_2 df(r,R_2,a_2)/dr, \qquad (5)$$

$$f(r,R_i,a_i) = \frac{1}{\{1+\exp[(r-R_i)/a_i]\}}. \qquad (6)$$

As shown in the inset of Fig. 2, they create two minima in the nuclear potential between ~ 5.5 fm and ~ 9.0 fm. The effect of these potentials can be understood in terms of the interference between the internal and barrier waves that correspond to a decomposition [24,25] of the scattering amplitude into two components, the inner and external waves. The inner wave comes from the reflection at the inner face of the total real potential pocket and the external wave comes from the reflection at the outer barrier (see Fig. 1 for the pocket in the total real potential). The presence of the two small potentials affects the phases and magnitudes of these internal and external components. We observe from the parameters in Table I that the two small additional potentials are not strong enough to produce pockets in the total real potential although they have a very significant effect on the scattering. This is demonstrated in Fig. 3 at 41.17 MeV. Figure 3(d) shows the cross sections obtained when both potentials are omitted. As a result, the calculated oscillations are out of phase with the measured ones even at the intermediate angles. Without these potentials, we were unable to refit the data by merely varying
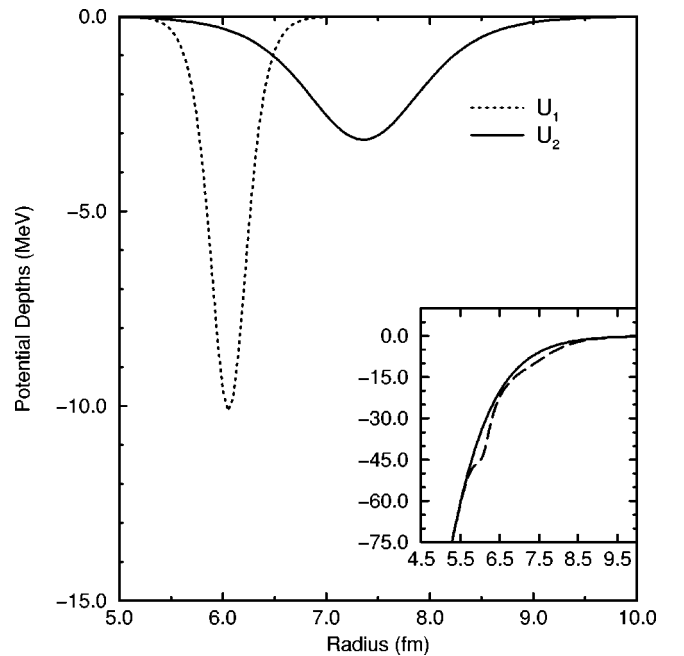

FIG. 2. The shapes of two small additional potentials U_1 and U_2 are displayed by dotted and solid lines, respectively. The inset shows their effects on the nuclear potential with a long-dashed line.
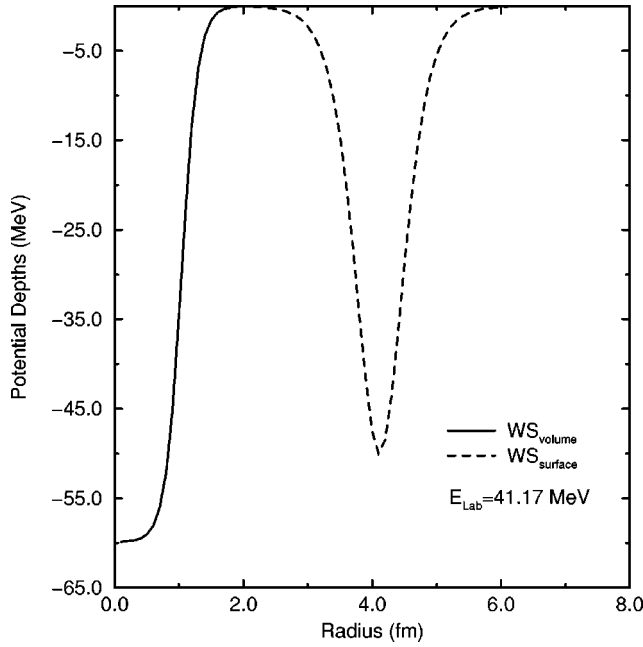
FIG. 3. The volume and the surface components of the imaginary potential at $E_{Lab}=41.17$ MeV for the ^{16}O+^{28}Si system.
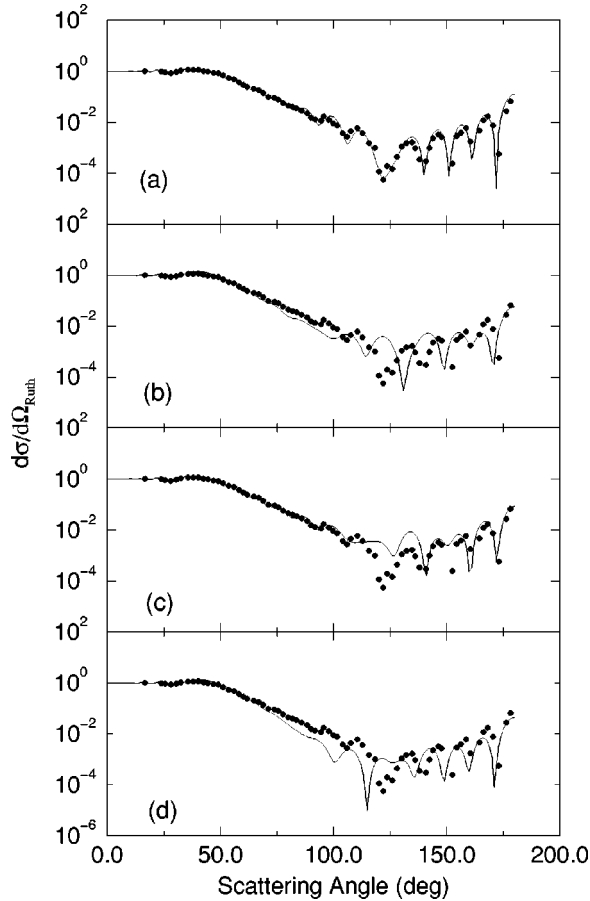

FIG. 4. The effect of the two small additional potentials for $E_{Lab}=41.17$ MeV. (a) reflects that the best fit is obtained with the inclusion of both potentials, (b) displays the situation without the inclusion of U_2 and (c) is without the inclusion of U_1. Finally, (d) displays the outcome when both potentials are ignored.
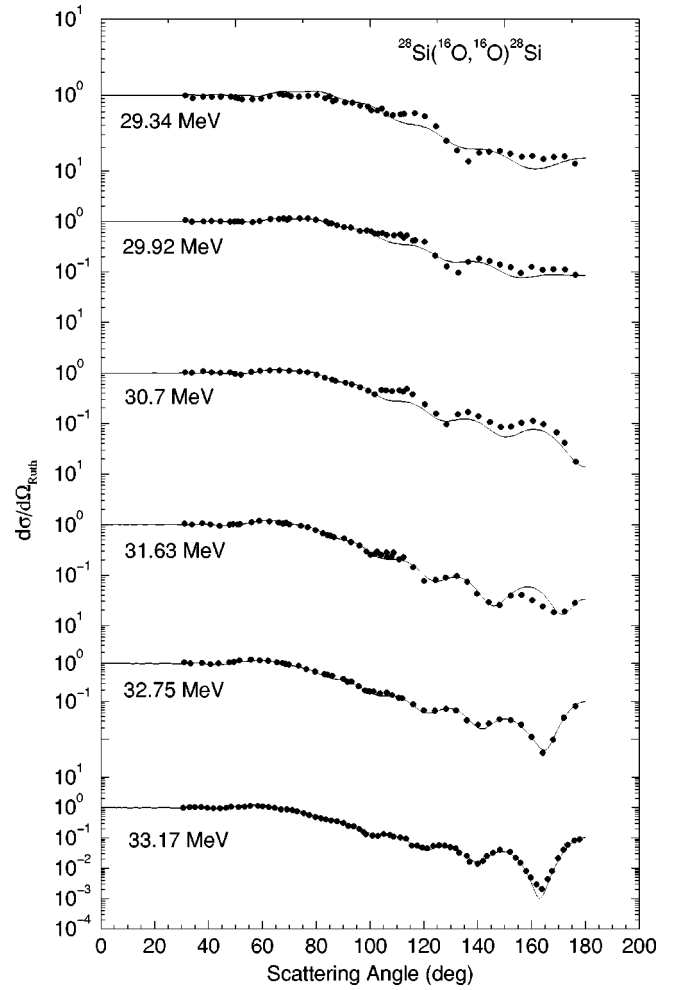

FIG. 5. The elastic scattering results obtained by using the single-channel optical model calculations for the ^{16}O+^{28}Si system.

the parameters of the real and imaginary potentials. Thus, the oscillatory structure could not be reproduced correctly.

The imaginary part of the potential was taken as the sum of a Woods-Saxon volume and the surface potential [19]:

$$W(r) = -W_V f(r,R_V,a_V) + 4W_S a_S df(r,R_S,a_S)/dr, \quad (7)$$

$$f(r,R,a) = \frac{1}{\{1+\exp[(r-R)/a]\}} \quad (8)$$

with $W_V=59.9$ MeV, $a_V=0.127$ fm, $W_S=50.0$ MeV, and $a_S=0.250$ fm. These parameters were also fixed in the calculations and only their radii were increased linearly with increasing energy according to the following formulas:

$$R_V = 0.060\,84 E_{CM} - 0.544, \quad (9)$$

$$R_S = 0.2406 E_{CM} - 2.191. \quad (10)$$

The imaginary potentials are shown in Fig. 4 for $E_{Lab} = 41.17$ MeV.

Moreover, the relative significance of the volume and surface components of the imaginary potential was evaluated for all the energies. For higher energies, omitting the volume
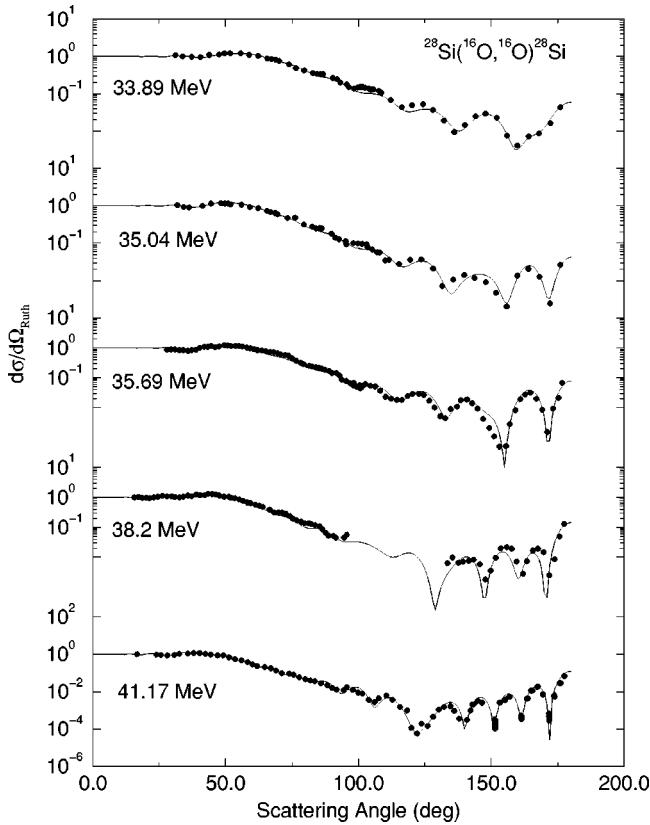
FIG. 6. Elastic scattering results obtained by using the single-channel optical model calculations for the $^{16}O + ^{28}Si$ system (continued from Fig. 5).

term predominantly affected the amplitude of the cross section at large angles. However, this effect was small and negligible at lower energies. Omitting the surface term increased the cross sections at large angles which were as much as two orders of magnitude. It was observed that this term had a significant effect at all the considered energies.

III. THE RESULTS

Using the above-described optical model with fixed real and linearly increasing imaginary potential parameters, we have analyzed the experimental data from 29.0 MeV to 142.5 MeV in the laboratory system. The comparisons between experimental data and the optical model fits are shown in Figs. 5–7. The χ^2 values for some of the energies studied are also shown in Table II. As it can be seen from these figures and the χ^2 table, we have obtained excellent agreement with the experimental data over the whole energy range considered.

We have also analyzed the averaged value of the excitation function over the angular range $180° \pm 5°$ with these potentials. The radii of the imaginary potential increased lin-

TABLE I. The parameters of the two small additional potentials.

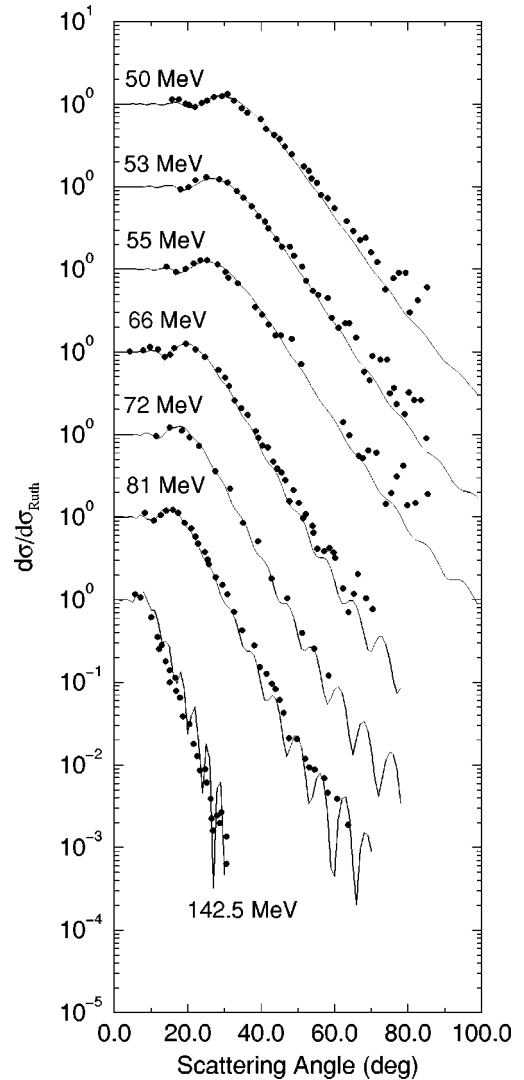| U_1 (MeV)	R_1 (fm)	a_1 (fm)	U_2 (MeV)	R_2 (fm)	a_2 (fm)
10.14	6.057	0.177	3.17	7.358	0.371

FIG. 7. Results of the elastic scattering calculation for forward angles at higher energies by using the single-channel optical model calculations.

TABLE II. χ^2 values for some of the energies studied.

Laboratory energy	Optical model
29.34	1.2
29.92	1.4
30.70	1.9
31.63	1.5
32.75	0.3
33.17	0.8
33.89	0.9
35.04	2.0
35.69	8.0
38.20	7.9
41.17	16.5

TABLE III. The parameters of the potentials required to fit the higher energy data. These are the values of the imaginary potential at $E_{Lab}=50$ MeV and they were fixed to reproduce the structure for forward angles at high energies for ^{16}O+^{28}Si.

W_V (MeV)	R_V (fm)	a_V (fm)	W_D (MeV)	R_D (fm)	a_D (fm)
59.90	1.3925	0.127	31.25	5.4697	0.550

early with energy up to 54.0 MeV according to Eqs. (9) and (10). Beyond this energy, we do not have the available experimental data for the large angles. Therefore, as shown in Table III, the radii were kept constant at that energy and were not changed for the higher energies. The result is compared with the measured values in Fig. 8. The overall agreement is quite good up to about 50 MeV where experimental data are available at large angles. In particular, the maxima and minima in the excitation function are obtained correctly. However, it should be emphasized that the calculated excitation function is much more sensitive to the details of the optical potential than are the fits to the angular distributions. For example, omitting two small potentials completely destroys the agreement with the excitation function.

We were able to obtain almost the same agreement with the experimental data above 50 MeV regardless of these two small potentials. This shows that for higher energies, the barrier/internal wave decomposition is not very important and thus we may remove these two small potentials. By using the same nuclear potential and the same type of imaginary potentials, but by readjusting the depth and diffuseness of its surface component, we were able to fit the experimental data from $E_{Lab}=50$ MeV to 142.5 MeV. These results are shown in Fig. 7 and the relevant parameters are shown in Table III.

IV. SUMMARY

We have shown a consistent description of the elastic scattering of the ^{16}O+^{28}Si system from 29.0 MeV to 142.5 MeV in the laboratory system by using the optical model calculations. In the introduction, we presented the problems that this reaction manifests. We attempted to find a consistent solution to these problems. However, within the standard optical model calculations, we failed, as others did, to describe certain aspects of the data.

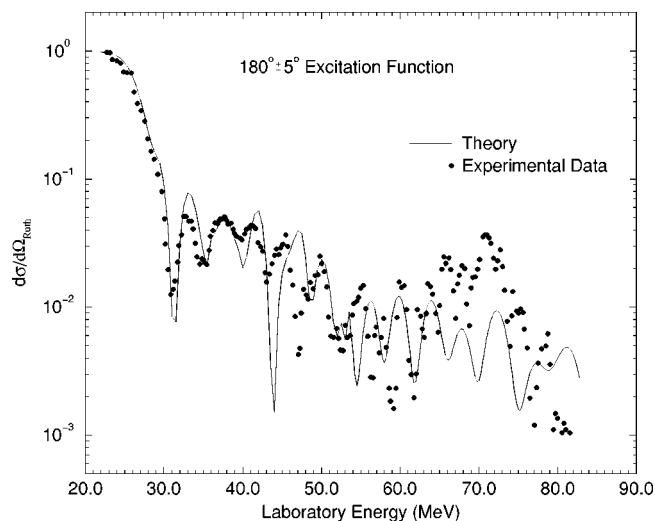Our previous elastic and inelastic analyses with light

FIG. 8. Comparison of the calculated 180° elastic scattering excitation function with the measured experimental data. The theoretical calculation is averaged over the last 5°.

heavy-ion reactions using the coupled-channels formalism had already shown that these reactions are extremely sensitive to the shape of the potential in the surface region. By taking this feature into account, we have used two small additional potentials that modify the shape of the potential in the surface region. As a result, we have obtained excellent agreement with the experimental data over a wide energy range similar to that of the coupled-channels method. The comparison of the results indicates that a global solution to the problems relating to the scattering observables of this reaction over a wide energy range has been provided by this method. Finally, it should be noted that although these additional two small potentials we used are very small and do not create a pocket in the total nuclear potential, they are very effective for the interference of the barrier and internal waves, which creates the oscillatory structure observed in the cross section. Further work in order to derive this term from a microscopic viewpoint is still under progress.

[1] P. Braun-Munzinger, G.M. Berkowitz, M. Gai, C.W. Jachcinski, T.R. Renner, C.D. Uhlhorn, J. Barrette, and M.J. LeVine, Phys. Rev. C **24**, 1010 (1981).

[2] P. Braun-Munzinger and J. Barrette, Phys. Rep. **87**, 209 (1982).

[3] W. Sciani, A. Lepine-Szily, F.R. Lichtenthaeler, P. Fachini, L.C. Gomes, G.F. Lima, M.M. Obuti, J.M. Oliveira, Jr., and A.C.C. Villari, Nucl. Phys. **A620**, 91 (1997).

[4] I. Boztosun and W.D.M. Rae, *Proceedings of the Seventh International Conference on Clustering Aspects of Nuclear Structure and Dynamics*, edited by M. Korolija, Z. Basrak, and R. Caplar (World-Scientific, Singapore, 2000).

[5] I. Boztosun, Ph.D. thesis, Oxford University, 2000.

[6] I. Boztosun and W.D.M. Rae, Phys. Rev. C **63**, 054607 (2001).

[7] I. Boztosun, Phys. At. Nucl. **65**, 607 (2002).

[8] I. Boztosun and W.D.M. Rae, Phys. Rev. C **65**, 024603 (2002).

[9] J. Barrette, M.J. LeVine, P. Braun-Munzinger, G.M. Berkowitz, M. Gai, J.M. Harris, and C.W. Jachcinski, Phys. Rev. Lett. **40**, 445 (1978).

[10] S. Kahana, B.T. Kim, and M. Mermaz, Phys. Rev. C **20**, 2124 (1979).

[11] D. Dehnhard, V. Shkolnik, and M.A. Franey, Phys. Rev. Lett. **40**, 1549 (1978).

[12] S. Kubono, P.D. Bond, and C.E. Thorn, Phys. Lett. **81B**, 140 (1979).

[13] G.R. Satchler, Nucl. Phys. **A279**, 493 (1977).

[14] K.O. Terenetski and J.D. Garrett, Phys. Rev. C **18**, 1944 (1978).

[15] T.R. Renner, J.P. Schiffer, D. Horn, G.C. Ball, and W.G. Davies, Phys. Rev. C **18**, 1927 (1978).

[16] S. Kahana, J. Barrette, B. Berthier, E. Chavez, A. Greiner, and M.C. Mermaz, Phys. Rev. C **28**, 1393 (1983).

[17] R.S. Mackintosh and A.M. Kobos, Phys. Rev. C **26**, 1766 (1982).

[18] A.M. Kobos, G.R. Satchler, and R.S. Mackintosh, Nucl. Phys. **A395**, 248 (1983).

[19] A.M. Kobos and G.R. Satchler, Nucl. Phys. **A427**, 589 (1984).

[20] I. Boztosun and W.D.M. Rae, Phys. Rev. C **64**, 054607 (2001).

[21] I. Boztosun and W.D.M. Rae, Phys. Lett. B **518**, 229 (2001).

[22] P.D. Kunz, computer code CHUCK.

[23] G.R. Satchler, *Direct Nuclear Reactions* (Oxford University Press, London, 1983); *Introduction to Nuclear Reactions* (Macmillan, New York, 1980).

[24] S.Y. Lee, Nucl. Phys. **A311**, 518 (1978).

[25] D.M. Brink and N. Takigawa, Nucl. Phys. **A279**, 159 (1977).